Results in Engineering 22 (2024) 101998

Contents lists available at ScienceDirect

Results in Engineering

journal homepage: www.sciencedirect.com/journal/results-in-engineering

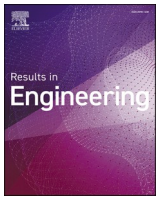

A new framework for improving MPPT algorithms through search space reduction

Ambe Harrison [a,*], Cyrille Feudjio [a], Christophe Raoul Fotso Mbobda [b], Njimboh Henry Alombah [c]

[a] Department of Electrical and Electronic Engineering, College of Technology (COT), University of Buea, Cameroon
[b] Department of Electrical and Electronic Engineering, National Higher Polytechnic Institute (NAHPI), University of Bamenda, Bambili, Cameroon
[c] Department of Electrical and Electronics Engineering, College of Technology, University of Bamenda, P.O. Box 39, Bambili, Cameroon

ARTICLE INFO

Keywords:
MPPT
Maximum power point (MPP) voltage
Search-space (SS)

ABSTRACT

In this article, a novel framework for improving maximum power point tracking (MPPT) is presented. A robust initialization of the MPPT algorithm is implemented, and the search space is reduced by rapidly predicting the maximum power point (MPP) voltage. In order to accomplish this, unknown parameters required to establish an empirical irradiance-free relationship between the open circuit voltage and MPP voltage were derived using three most prevalent PV panel models. The P&O MPPT algorithm implements this framework, which establishes a systematic boundary to confine the MPP voltage to a reduced search space by virtue of this relationship. The evaluations performed on three distinct varieties of commercial PV panels demonstrated that the PV panels modeled in this study exhibit a high degree of conformity with the data provided by the manufacturers. Furthermore, the estimation of MPP voltage allows for a reduction of the search space by as much as 2% of its initial area. The efficacy of the proposed MPPT algorithm is found to be 96.64%, higher than that of the P&O and other implemented contemporary algorithms, when evaluated against a common platform and rapidly changing climatic conditions. Real-world climatic experiments are performed in order to assess the feasibility of the established research. The experimental results indicate that the established irradiance-free MPP voltage has a mean error of merely 0.0128V. Furthermore, the combined output power generated by the MPPT proposed algorithm under experimental conditions is comparatively superior in performance.

1. Introduction

The transition to renewable energy sources (RSEs) is an essential remedy for the world's environmental challenges, such as climate change and global warming, of which fossil fuels comprise approximately 81% of primary energy sources [1–4]. Over the course of the last decade, numerous RSEs have been examined with the intention of mitigating these environmental concerns; solar energy has emerged as a particularly dependable option [1,5]. Consequently, solar photovoltaic (PV) systems have experienced a substantial surge in research and development over the past few years [6]. Notwithstanding this discernible advancement, photovoltaic solar panels continue to exhibit an exceptionally low conversion efficiency [7]. Furthermore, the PV module produces a power output that exhibits nonlinearity and varies in response to environmental factors [8]. These fluctuations diminish the PV panel's operational capacity, resulting in the operating power failing to correspond with the maximum power point (MPP). Consequently, the MPP is distinct for each environmental configuration (temperature and irradiance). In order to address this issue, it is crucial to implement a mechanism called the maximum power point tracking (MPPT) algorithm, which compels the PV module to consistently produce its maximum energy output [8].

Prominent works in the field of MPPT encompass a diverse array of algorithms, each distinguished by its cost, operational range, tracking speed, intricacy, and number of required sensors [9]. Nevertheless, these MPPT algorithms are ineffective in accurately tracking the maximum power point (MPP) due to the extensive operating range. This lack of efficiency hinders rapid convergence around the MPP, resulting in steady-state oscillations. Certain basic methods, like the fractional open-circuit voltage (FOCV) [10], are easy to apply. However, they rely on estimating the open circuit voltage [11] of the PV module and do not accurately track the genuine maximum power point (MPP) of the panel.

* Corresponding author.
E-mail address: ambe.harrison@ubuea.cm (A. Harrison).

https://doi.org/10.1016/j.rineng.2024.101998
Received 8 November 2023; Received in revised form 21 December 2023; Accepted 8 March 2024
Available online 15 March 2024

This is because the MPP voltage is only approximated from the open circuit voltage. The fractional short-circuit current (FSCC) [10], has emerged as an alternative method to the FOCV. It relies on the approximate relation between the short-circuit current of the panel and the MPP current but suffers from similar limitations as the FOCV method. The pilot cells method [12] has emerged as an improvement to the FOCV/FSCC method as it gets rid of periodical disconnection to measure the open-circuit voltage or short-circuit current. Although this method handles power loss issues, it does not track the true MPP voltage because it still relies on its approximation.

As opposed to approximate estimation methods, searching algorithms are frequently used to monitor the MPP voltage. Given the circumstances, numerous MPPT searching algorithms have been suggested in scholarly works, with the P&O algorithm being the most widely used and most straightforward [13–15]. By continuously varying or perturbing the voltage until the operating point reaches the MPP, the P&O meticulously searches for the MPP within the power-voltage (P–V) curve. Proximities of this nature have the potential to generate oscillations in the vicinity of the MPP, consequently diminishing the operational efficiency of the PV system [13]. The algorithm is, in fact, forced to strike a balance between monitoring speed and oscillations around the MPP. A larger step size of perturbation results in reduced oscillations around the MPP, which hinders tracking speed and accuracy. Conversely, an increase in step size of perturbation enhances tracking speed but at the cost of oscillations. In summary, the algorithm's overall efficiency is constrained, but a prudent choice of step size perturbation accomplishes a satisfactory compromise between tracking speed and accuracy [13]. In Ref. [16], a variable step-size P&O was proposed to automatically adjust the perturbation size according to the operating point. Such auto-adjustment of the perturbation step size is bound to achieve moderate performance if the search space for the MPP voltage is the entire PV curve. To alleviate this problem, a beta MPPT algorithm was proposed [17,18] by introducing a new parameter "beta" to ensure an injective relationship with the power. However, this method adequately addresses the trade-off problem only when the panel operates within a restricted range of temperature and irradiance.

In recent times, scholars have begun to focus on the optimization of MPPT algorithms via the diminution of the MPP's search space. Indeed, the inefficiency of certain MPPT algorithms can be attributed to the substantial area needed to target the MPP, which consequently hampers the monitoring process. However, in regard to practical implementation, this matter remains arduous to resolve. As prospective solutions to MPPT, intelligent optimization algorithms including fuzzy logic control (FLC) and artificial neural networks (ANN) have surfaced. Relying on FLC to determine the step-size of the searching algorithm can alleviate the limitations of the P&O [19,20]. In Ref. [21], a hybrid adaptive reference calculation and FLC is suggested, in which the determination of the reference voltage is heavily dependent on solar irradiance measurements. The FLC subsequently determines the control duty cycle of the algorithm. While this strategy is more efficient than the P&O, its practical implementation in a PV system is complicated due to the requirement of measuring solar irradiance. An additional limitation of the FLS method is its heavy reliance on the designer's knowledge of fuzzy systems principles [22]. Various scholars have introduced different modifications to the P&O and other approaches inspired from intelligent, fuzzy and nonlinear control to improve the performance of MPPT algorithms [23–30]. Numerous alternative strategies have been investigated in an effort to improve the performance of PV systems in both grid-connected and off-grid connected configurations. A modified shuffled frog optimized fuzzy logic MPPT algorithm for a PV-grid connected system with battery storage was suggested [31]. In Refs. [32,33], climatic sensor dependent intelligent approaches adapted to classical ANN and ANFIS were studied to improve the performance of PV systems. A major shortcoming of such climatic sensor approaches lies in the huge burden of integrating climatic sensors in the PV systems such as the Pyranometer [34]. Alternatively, focusing on simplicity, an optimized fractional short circuit method was proposed to regulate the PV system and attain MPPT in an optimal way. It is also noteworthy that the PV is a nonlinear system with some degree of fractionality, which was handled by the combined operation of a fractional P&O and a fractional PI controller [35]. To circumvent the need of optimal determination of fractional order parameters, the latter work resorted to the Hunter-Prey optimization algorithm. When considering operating conditions such as load, temperature, and irradiance, the fractional MPPT system dynamically possesses an additional degree of freedom that improves its operational range relative to the classical PI controller. Nonetheless, overall system optimality may only be applicable to the operating conditions for which the optimal parameter was derived, despite the fact that the three parameters of the fractional order PI controller are determined by a well-behaved optimization algorithm. Thus, in operating regions far from the optimization setting, the overall performance of the PV system is susceptible to depreciation.

The potency of MPPT to minimize PV power losses and provision of operational stability under severe weather conditions was investigates in Ref. [36], while in Ref. [37], authors studied collaborative algorithms (fuzzy logic and sliding mode controller) to demonstrate how optimal operation and cost minimization can be achieved in a single stage grid-connected PV system. In summary, the literature has documented a multitude of contributions aimed at enhancing the MPPT algorithms. These contributions are succinctly outlined in Table 1.

As it can be noticed in Table 1, a good number of these algorithms rely on the measurement of solar irradiance that is expensive and complex to integrate in an MPPT algorithm. Other MPPT methods are based on nonlinear control [30] with higher order of complexity,

Table 1
Summary of other contributions to MPPT in PV systems.

Ref	Year	Specificity	Sensors used	Key Remarks
[17]	2015	Beta Algorithm	Current, Voltage	- Temperature variations not considered. - Restricted operating range (300-1000 W /m^2).
[23]	2018	Hybrid Fuzzy Logic	Current, Voltage	- Complex fuzzy rules - Required good knowledge fuzzy rules design
[24]	2019	Adaptive Variable Step Size	Current, Voltage	- Multi-stage parameters to determine - Trade-off problem
[25]	2018	Artificial neural network	Current, Voltage, Irradiance, Temperature	- Complex implementation - Low feasibility due to neural network size
[30]	2018	Nonlinear back-stepping algorithm	Current, Voltage, Irradiance, Temperature	- Complex implementation - Internal and dynamics of the system are subjective
[27]	2020	Hybrid PSO and Artificial neural network	Current, Voltage, Irradiance, Temperature	- Complex implementation due to the complex structure of ANN (18 neurons in hidden layer) - Requires irradiance measurement
[28]	2018	Confined search space	Current, Voltage	- Search space based on subjective assumptions
[29]	2021	Search space	Current, Voltage	- Search space based on subjective assumptions
[38]	2023	PSO trained machine learning and Flying Squirrel search Optimization	Current, Voltage, Irradiance, Temperature	- Complex implementation - Requires irradiance measurement - Very low convergence speed due to large search space

requiring the determination of the full dynamics of the PV system which is not always available. Some algorithms attempt to consolidate the simplicity while addressing the main limitations of the P&O [17,28]. However, they still suffer major setbacks leading to moderate performance because of the large size of the search space (SP). The power-voltage curve of a PV panel under standard test condition is shown in Fig. 1.

From the zero voltage point (ZVP) to the open circuit voltage point (OCVP), he P&O and other algorithms are specifically engineered to locate the MPP across the entire P–V curve. Conducting a search operation across the entire curve inevitably causes a deceleration in the algorithm's response tine and yields a moderate level of operating efficiency. Consequently, the aforementioned constrains will be alleviated and the algorithm's efficacy enhanced by minimizing this search space (SS). Given this perspective, certain authors postulated that the MPP consistently occupied the region between 70% and 80% of the P–V curve, predicated on the inherent correlation between the open circuit voltage and the MPP voltage [28]. As a results, a 10% selected area in the initial SS was achieved. It should be noted that, however, that the open circuit voltage fluctuates when the PV panel is exposed to climatic changes, md the confined SS may not always locate the actual MPP. As a result, the algorithm's ability to monitor the effective and accurate MPP may be contingent. Thus, developing a method that precisely and methodically delineates the reduced search space (RSS) containing the MPP, regardless of climatic fluctuations, is a practical approach to addressing this issue.

Therefore, in this paper, a novel comprehensive MPPT framework is presented, which integrates search space reduction with MPP voltage estimation. In order to estimate the MPP voltage while resolving implementation-related challenges, an empirical relationship between the open circuit voltage and the MPP voltage was established using an irradiance-free equation. Utilizing experimental data supplied by the manufacturer of three primary varieties of solar panels—multi-crystal KC200GT, poly-crystalline MSX-60, and mono-crystalline CS6K-280M—the validity of this method is established. The excellent precision of the approximated MPP voltage enables the RSS limits, which form the foundation of the newly introduced MPP framework, to be determined with dependability. Finally, the assessment and comparison of the proposed strategy to those of the state-of-the-art algorithms including the standard P&O, confine search space algorithm developed in Ref. [28], and the MPPT strategy in Ref. [29] are carried out to assess its performances in terms of tracking response and power extracted. The main contributions of this work can be summarized as follows.

- ❖ Establishment of a simple straightforward equation between the open circuit and MPP voltage
- ❖ Validation of the proposed equation on three solar panels
- ❖ Introduction of a precise and systematic approach for determining the bounds of the reduced search space
- ❖ Development of a new comprehensive algorithm by leveraging MPP voltage estimation and reduced search space tracking of the MPP

The subsequent sections are structured as follows: The foundation of a typical PV system under investigation is briefly described in Section 2, whereas the PV panel modeling strategy is introduced in Section 3. In section 4, the equation utilized to calculate the MPP voltage and RSS is presented. The new framework for the modified MPP algorithm is presented in Section 5. The findings of this investigation are detailed and analyzed in Section 6 as well as comparisons with state-of-the-art algorithms. The paper is concluded in Section 7.

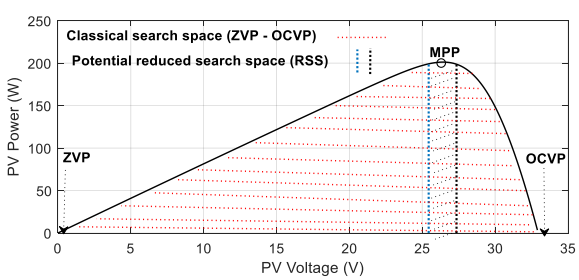

Fig. 1. Power-Voltage curve of a PV panel.

2. Brief overview on PV system

A typical PV connected system (PVCS) consists of a solar PV panel coupled to a DC load through a DC-DC boost converter. Note that the investigations carried out in this paper do not cover PV connected system under partial shading conditions but rather assumes uniform distribution of sun irradiance on PV module [8]. The boost converter is the most popular DC-DC converter in which MPPT algorithms have been implemented [39]. In the MPPT context, boost converter is chosen for its high gain and efficiency in comparison to other DC-DC converters such as Buck converter [40]. Maximum power transmission to the load is achieved through the implementation of a boost converter in this design. In accordance with the current PV output ratings, the MPPT algorithm must operate the boost converter at the proper duty ratio in order to accomplish this. To ensure the DC-DC converter operates efficiently, the MPPT block must promptly update the duty ratio in response to the output parameters (voltage and current) of the PV module. Unfortunate as it may be, the algorithm's efficacy in monitoring the MPP diminishes as its complexity increases, particularly when confronted with fluctuating environmental conditions, and the latency in updating the duty ratio increases. In the case of the P&O algorithm, one of the most widely used MPPT algorithms, this circumstance becomes complex when the MPP is sought across the entire P–V curve. Restricting the search space for the MPP and implementing a robust initialization to accelerate the algorithm is one method to mitigate this issue.

In an effort to identify potential enhancements by reducing the search space, this article reconsiders the framework of MPPT algorithms. In pursuit of this objective, a methodology is formulated to restrict the range of possible MPP voltage values by establishing a correlation between the open circuit voltage and the MPP voltage. It is important to mention that the open circuit voltage at the PV panel's output can be mathematically described using a suitable model of the PV panel. The literature contains numerous PV panel models, with the single diode, double diode, and three diode configurations being the most widely used [41–43]. However, the single-diode model is the most used because of its reasonable balance between complexity and performance [44]. To this extend, in this paper, the PV panel is modeled using the single diode model to satisfy the constraints of the monocrystalline, polycrystalline, and Multicrystalline PV panels. Thanks to this PV panel modelling, a straightforward equation between Voc and Vmpp will be established. Finally, the confined search space developed is applied to the conventional P&O MPPT algorithm to assess improvements achieved with such a strategy to the performances of this algorithm.

3. Modelling of the solar panel

Fig. 2 depicts the single-diode model of the solar panel.

This model is made up of an ideal current source I_{ph}, a parallel diode (D_1), and a parallel and a series resistances respectively (R_p) and (R_s). The current source delivers a photocurrent current, which is proportional to the solar irradiance (G) and proportional to the temperature (T). The diode models the semi-conducting effect of the PV panel and emulates the nonlinear features of the cell. The resistances R_p, and R_s models the ohmic losses of the semiconductor material. Applying the Kirchhoff's current law to the circuit of Fig. 4, the current I_{pv} of a cell can be expressed mathematically as:

$$I_{pv} = I_{ph} - I_{D1} - I_{Rp} \quad (1)$$

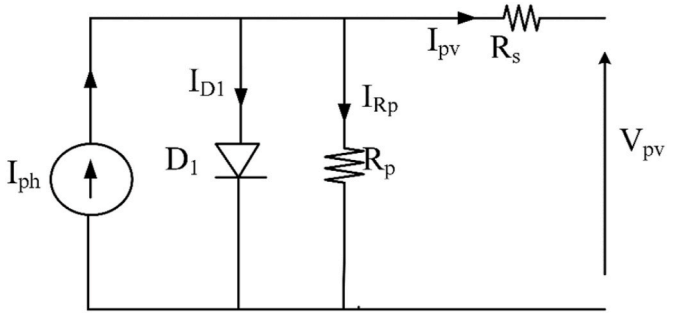

Fig. 2. Single diode model of the solar panel.

where I_{ph} is the photocurrent of the current source, I_{D1} is the current through diode D_1 and I_{Rp} is the current through the parallel resistance R_p. Using the diode current expression and applying Ohm's law across R_p equation (1) is rewritten as:

$$I_{pv} = I_{ph} - I_s\left(e^{\frac{V_{D1}}{nN_sV_t}} - 1\right) - \frac{V_{D1}}{R_p} \tag{2}$$

where V_{D1} is the voltage across diode D_1, $I_{D1} = I_s\left(e^{\frac{V_{D1}}{nN_sV_t}} - 1\right)$ is the diode current flowing in D_1, n is the ideality coefficient of the diode, N_s the number of cells and V_t is the thermal voltage of the cell expressed as $V_t = \frac{K_BT}{q}$, where K_B is the Boltzmann constant and q is the electric charge. Note that $I_{Rp} = \frac{V_{D1}}{R_p}$, $V_{D1} = V_{pv} + I_{pv}R_s$. With all of the above, Equation (2) can be expressed as:

$$I_{pv} = I_{ph} - I_s\left(e^{\frac{V_{pv}+I_{pv}R_s}{nN_sV_t}} - 1\right) - \frac{V_{pv} + I_{pv}R_s}{R_p} \tag{3}$$

Equation (3) exhibits the nonlinear relationship of the current-voltage of the cell. From this equation, the following five parameters $I_{ph}, I_s, n, R_p,$ and R_s are necessary for a complete modelling of PV panel. Such a modelling is vital for a comprehensive assessment of the MPPT algorithms under uncontrolled environmental conditions. With an accurate model of the PV in hands, one can thoroughly study its operation under diverse environmental conditions. This paper puts forward a hybrid analytical and particle swam optimization (PSO) method to accurately identify these unknown parameters by relying on some PV panel quantities that are available or can be computed easily.

Assuming the PV module in open circuit state, the current I_{pv} is zero and the PV voltage is the open-circuit voltage V_{oc}. Under this condition, Equation (3) becomes:

$$0 = I_{ph} - I_s\left(e^{\frac{V_{oc}}{nN_sV_t}} - 1\right) - \frac{V_{oc}}{R_p} \tag{4}$$

and the photocurrent I_{ph} is expressed as:

$$I_{ph} = \frac{V_{oc}}{R_p} + I_s\left(e^{\frac{V_{oc}}{nN_sV_t}} - 1\right) \tag{5}$$

Similarly, short-circuiting the PV module, V_{pv} becomes zero and I_{pv} becomes equal to the short circuit current, and Equation (3) becomes:

$$I_{sc} = I_{ph} - I_s\left(e^{\frac{I_{sc}R_s}{nN_sV_t}} - 1\right) - \frac{I_{sc}R_s}{R_p} \tag{6}$$

Note that at the maximum power point (MPP), the PV current and voltage are given by I_m, V_m respectively and applying this proposition to Equation (3) gives:

$$I_m = I_{ph} - I_s\left(e^{\frac{V_m+I_mR_s}{nN_sV_t}} - 1\right) - \frac{V_m + I_mR_s}{R_p} \tag{7}$$

So that the maximum power ($P_m = V_mI_m$) can be expressed as

$$P_m = V_m\left(I_{ph} - I_s\left(e^{\frac{V_m+I_mR_s}{nN_sV_t}} - 1\right) - \frac{V_m + I_mR_s}{R_p}\right) \tag{8}$$

Note that the values of the parameters I_m, P_m, V_m, V_{oc} and I_{sc} are given at standard test conditions (STC) and provided by the manufacturer of the PV panel in the datasheet, or user manual or nameplate of the PV module. As a result, this latter can be effectively exploited to derive the unknown parameters of the PV module. For practical implementation, the previous parameters are computed even for conditions other than STC, the quantity I_{ph} is computed while the other four ($I_s, n, R_p,$ and R_s), will be derived using PSO.

3.1. Computation of the unknown parameters of the PV panel

Particle swarm optimization (PSO) algorithm [45] is a population-based intelligent algorithm that falls under the umbrella of optimization algorithms called metaheuristics. It is a biologically inspired algorithm from animal social behavior such as fish and birds [46]. It has been applied to solve various engineering optimization problems [38]. In this realm, a set of particles in a given region or space, sail towards a destination by searching for the shortest path. The best solution is achieved through social cooperation and transfer learning from the particles in the search space. The PSO algorithm is governed by the velocity and position of every particle which is described by the following equations [45]:

$$x_{ij}^{n+1} = x_{ij}^n + v_{ij}^{n+1} \tag{9}$$

$$v_{ij}^{n+1} = \omega v_{ij}^n + r_1c_1\left(p_{ij}^n - x_{ij}^n\right) + r_2c_2\left(g_{ij}^n - x_{ij}^n\right) \tag{10}$$

where $x_{ij}^{n+1}, v_{ij}^{n+1}$, are the position and velocity of the particle i at the $(n+1)^{th}$ iteration in the j dimension. ω is the inertia weight, c_1, c_2 are the self-weight and social learning coefficient respectively. r_1 and r_2, are uniformly distributed random numbers between 0 and 1. p_{ij}^n, is the best position of the best particle in the j dimension evaluated at the n^{th}, while g_{ij}^n is the global best position. The optimization task is achieved by minimizing the objective function

$$F_{min} = e_1 + e_2 + e_3 \tag{11}$$

where $e_1 = |I_{m-com} - I_{m-datasheet}|$, $e_2 = |I_{sc-com} - I_{sc-datasheet}|$, and $e_3 = |P_{m-com} - P_{m-datasheet}|$. Note that, I_{m-com} is the computed maximum current (I_m) evaluated by Equation (7). $I_{m-datasheet}$, $I_{sc-datasheet}$, and $P_{m-datasheet}$ are respectively the maximum current, short-circuit current and maximum power provided by manufacturer in the datasheet of the solar panel. I_{sc-com} is the computed I_{sc} from Equation (6) and P_{m-com} the computed P_m from Equation (8). Practically speaking, the optimization algorithm attempts to minimize the errors between the computed parameters from those provided in the datasheet. At the convergence, the algorithm provides the best values for the parameters $I_{ph}, I_s, n, R_p,$ and R_s.

The following parameters of the PV model are defined at environmental conditions different from those of standard test conditions (STC) [41] as:

$$I_s = I_{s-STC}\left(\frac{T}{T_{STC}}\right)^3 e^{\frac{qE_g}{nK_B}\left(\frac{1}{T_{STC}} - \frac{1}{T}\right)} \tag{12}$$

$$E_g = E_{g-STC}(1 - 0.0002677)(T - T_{STC}) \tag{13}$$

$$R_p = R_{p-STC}\, G_{STC} / G \tag{14}$$

$$I_{ph} = \left(I_{ph-STC} + K_i(T - T_{STC})\right) G_{STC} / G \tag{15}$$

where E_g is the bandgap energy of the PV cell, and K_i is the temperature

coefficient of short-circuit current. The subscript parameter "STC" specifies a parameter obtained at STC. Once the five parameters are identified, they are fed back into the model as shown in Fig. 5 for subsequent MPPT investigations.

4. Estimation of the MPP voltage

At this stage, a simple equation is put forward to enable a rapid determination of the MPP voltage. Several related scientific literatures have attempted to formulate equations to determine or estimate of MPP voltage. One of the most common approaches is based on the FOCV method [11] that relates the open-circuit voltage to the MPP voltage as follows:

$$V_m = A_v V_{oc} \tag{16}$$

Equation (16) translates a simple linear relationship between the MPP voltage V_m and V_{oc} with A_v admitting a constant value that depends on the solar panel. Another version of this linear relationship was formulated in Ref. [47] as:

$$V_m = A_v V_{oc} + C \tag{17}$$

It can be noticed in these two equation that the estimation of V_m relies on the measurement of open circuit voltage. In practical settings, this requires a brief disconnection of the PV panel from the system to measure V_{oc} thereby inducing energy losses. In addition, the accuracy in V_m dependents on appropriate determination of the constant A_v. Unfortunately, this coefficient is subject to variation with the environmental conditions such as irradiance and temperature. Fig. 3 shows a scattered plot of V_m against V_{oc} with V_{oc} obtained through simulations for the model with a mapping of irradiance and temperature in the range [0–1000W/m^2] and [0-75 °C] respectively. The line in dots fitted in the scattered point was obtained by performing a linear fitting. It is obvious that relation between V_{oc} and V_m is not linear. Furthermore, the random gaps observed between the lines suggests different values of A_v and C. As a result, a simple linear model cannot represent the relationship between V_m and V_{oc}. To address this problem, some authors developed an approach relying on an offline look-up table (LUT) using extra pilot solar panels and genetic algorithm [48]. Although, this approach could produce accurate results, the restricted range of the LUT added to its complexity make its integration ineffective into a PV system. Several other methods have been proposed in the literature to quickly estimate the MPP voltage including mathematical regression plane [30] which is defined by the following equation:

$$V_m = a + bT + cG \tag{18}$$

where G, T are the solar irradiance and temperature. The coefficients a, b, c are some offline pre-determined constants. Such an approach relies on more sensors (irradiance and temperature) and is still difficult to implement in a PV system because of the complexity in measuring solar irradiance. Finally, a way around this problem for quick estimate of V_m is to get rid of sensors and rely on a simple and straightforward

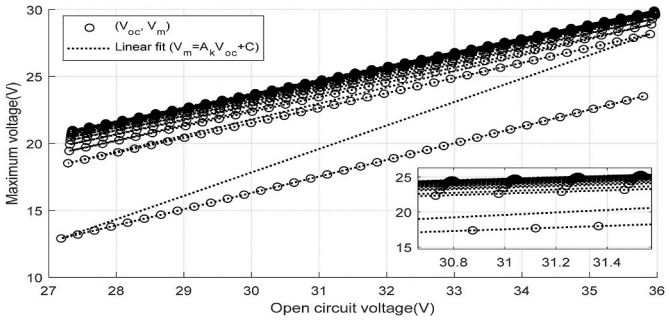

Fig. 3. Relation between V_{oc} and V_m.

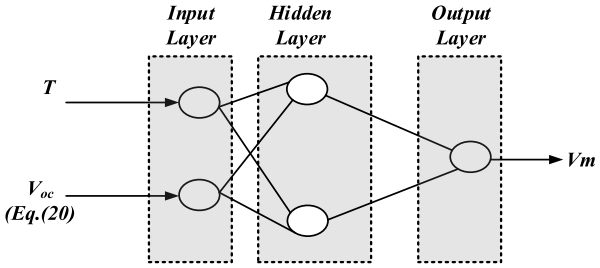

Fig. 4. Structure of the proposed ANN.

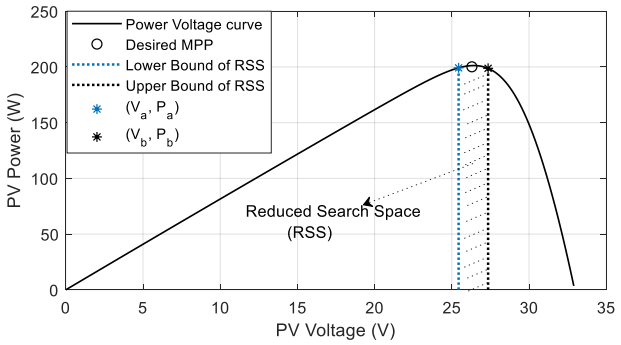

Fig. 5. Reduced search space delineation on Power-Voltage curve of a PV module.

equations to estimate the MPP voltage.

4.1. Fast estimation of the MPP voltage

According to the Sandia National PV modeling laboratory and in conformity with [49], the open circuit voltage of the panel can be computed straightforward using the following equation:

$$V_{oc} = V_{oc-STC} + nV_t In\left(\frac{G}{G_{STC}}\right) + K_v(T - T_{STC}) \tag{19}$$

where K_v is the temperature coefficient of open circuit voltage. Note that this constant can be made available by the manufacturer or from the modelling. Nevertheless, the irradiance parameter is still a burden for its practical implementation. One can easily get rid of it by combining Equations (15) and (19) to obtain:

$$V_{oc} = V_{oc-STC} + nV_t In\left(\frac{I_{pv}}{I_{ph-STC} + K_i(T - T_{STC})}\right) + K_v(T - T_{STC}) \tag{20}$$

The term I_{ph-STC} is derived from the PV model directly after the determination of the unknown parameters with PSO. It should be noted that while the expression of V_{oc} is now devoid of irradiance at this level, its evaluation necessitates the temperature and current of the PV module, which are readily obtainable.

As shown in Fig. 3, the non-linear behavior of V_m with regard to environmental conditions can only be modeled by a non-linear system such as an artificial neural network (ANN). The general theory of ANN has already been well documented in the literature [50,51]. ANN are biologically inspired computational networks that mimics the intelligence of the human brain. They belong to the class of machine learning algorithm that are trained to self-recognize prominent patterns from a dataset that well describes the system producing those data. In this paper, for the sake of system simplicity and effectiveness, a simplest feed forward neural network made up of two inputs, one hidden layer and a single output is considered. The inputs are fed by the parameters T and V_{oc}, while the output produces V_m. The hidden layer is made up of only

two neurons to minimize the network complexity. The architecture of the proposed ANN used to estimate of the MPP voltage using V_{oc} and T respectively is shown in Fig. 4.

5. Improving MPPT algorithm through search space reduction using V_m estimation

It is essential to remember that the objective of every MPPT algorithm is to precisely calculate V_m so that the MPP can be obtained. The preceding section described a methodology for estimating V_m via ANN. While such an approximation may be reasonably precise, the ANN is not always capable of predicting the exact value of V_m due to the logistic regression nature of the task and the model's limitations, which introduce some bias into the value of V_m. As a result, the estimated V_m is not regarded as the MPP in this paper; instead, it is utilized to reduce the search space and enhance the efficacy of the MPPT algorithms. To achieve this, a methodical approach to search space reduction is devised and subsequently incorporated into the conventional P&O algorithm. The efficacy of this approach is evaluated through a series of experiments.

On the PV power-voltage curve, the MPP is found at the apex of the curve as illustrated in Fig. 5. Thanks to the estimated V_m, the desired MPP can be accurately confined within well-known space. In some works [28,29], this confinement process was done on subjective grounds. This paper introduces a methodical and systematic approach for determining the bounds of the reduced search space (RSS). With the estimated V_m in hands, the upper bounds and lower bound respectively V_a, and V_b of the RSS as shown in Fig. 5 can be defined as:

$$V_a = V_m - |\varepsilon_a| \tag{21}$$

$$V_b = V_m + |\varepsilon_b| \tag{22}$$

where ε_a and ε_b represent respectively the maximum upper and lower deviation observed on the estimated V_m during the testing stage of the neural network.

The improved MPPT algorithm introduced in this paper is summarized by the flowchart depicted in Fig. 6. The PV voltage, current and temperature are obtained from sensors, V_{oc} is computed using Equation (20) and fed to the ANN that provides V_m that is then used to set the lower and upper bound of the RSS V_a and V_b using Equations (21) and (22). These parameters are used as inputs of the MPPT algorithm. Roughly speaking, an efficient implementation of the RSS in an MPPT algorithm imposes the operating point (initially V_{pv}) to be located within the confined space. However, such a constraint is not always met especially when the PV panel is subject to load variations or changes in environmental conditions. To make sure that such a constraint is always satisfied, a robust initialization stage is developed to ensure that the operating point is found within the RSS region before deploying the MPPT algorithm.

The goal of the initialization stage is the dynamic adjustment of the duty cycle to drive quickly the operating point into the RSS region. Whenever V_{pv} is lower than or equal to V_a, the duty cycle is reduced from its previous value to allow the operating point to enter the RSS region. Otherwise, if V_{pv} is greater than V_b, the duty cycle is increased to bring back the operating point within the RSS region. The modification on duty cycle during this initialization stage are by the following equations:

$$D(k+1) = D(k) - K_\tau \left| V_{pv}(k) - V_a \right| \tag{23}$$

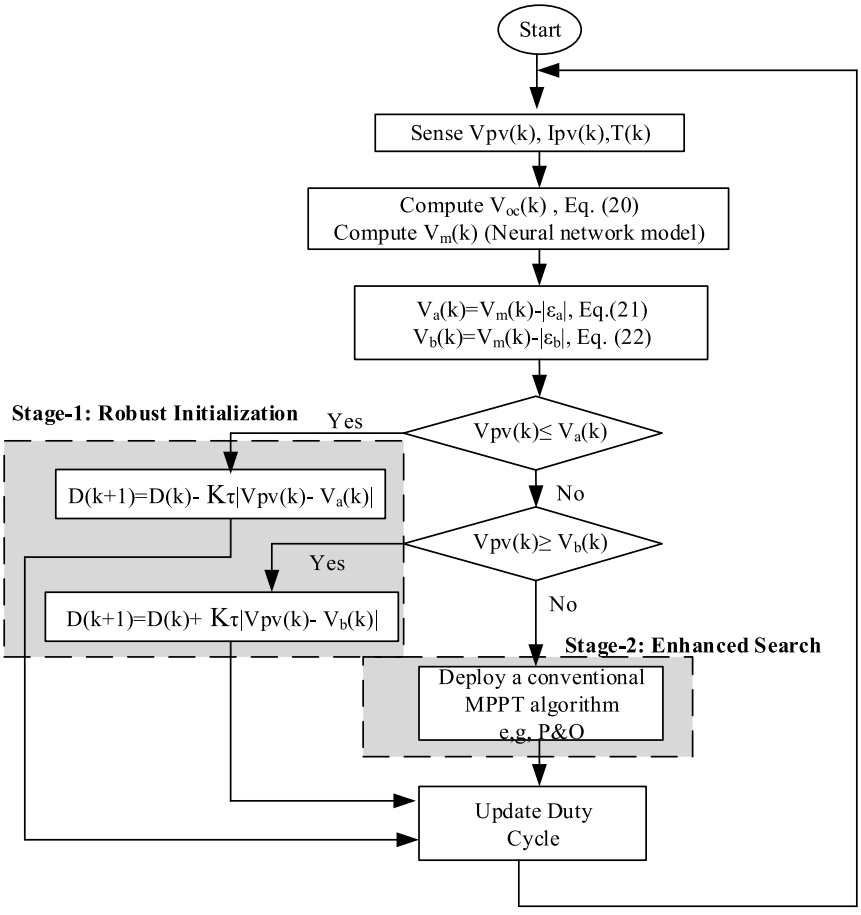

Fig. 6. Flowchart of the improved MPPT Algorithm.

$$D(k+1) = D(k) + K_\tau \left| V_{pv}(k) - V_b \right| \quad (24)$$

where D(k) and D(k+1) are the duty-cycle perturbation at the kth and $(k+1)^{th}$ instant.

The parameter K_τ plays an important role in the robust initialization. It is chosen in such a way to enable the algorithm to drive rapidly the operating point into the RSS in a reduced number of step. For a fast and reliable response of the algorithm, K_τ adapt the duty cycle with respect to the difference between the PV operating point and the RSS bounds ($\left| V_{pv}(k) - V_a \right|$). Once the operating point is brought into the RSS Region, the MPPT algorithm takes over. The RSS enhances the MPPT algorithm by speeding up the convergence to the MPP and the choice of the P&O perturbation parameter ΔD is based on the minimization of the oscillations around the MPP

6. Results

In this section, series of experiments were conducted under diverse environmental conditions to first of all assess the accuracy and performances of the solar panel model then the efficiency of the improved MPPT algorithm. Subsequently, the performances of the proposed algorithm are presented and compared to those of the conventional P&O algorithm and as well as to some state-of-the-art methods [28,29]. Finally, a discussion is carried out on the relevance of the modified MPPT algorithm and on experimental results obtained from real-time data.

6.1. Assessment of the PV panel modelling

The PV panel modeled was assessed using three main classes of commercial solar panels, namely, multicrystal KC200GT, poly-crystalline MSX-60, and mono-crystalline CS6K-280 M. The specifications of these panels are presented in Table .2. The five unknown parameters of the single diode model obtained through minimization of the PSO fitness function (Eq. (11)). The constant parameters c_1, c_2, and ω used for the implementation of the PSO algorithm were found to produce optimal results for $c_1 = c_2 = 1.4962$, and $\omega = 0.7298$.

The PSO algorithm was implemented for a maximum of 1000 iterations. The fitness curves for the PV panel types KC200GT, MSX-60, and CS6K-280 M displayed in Fig. 7 shows a fast decay towards a minimum value close to zero. At the minimum point, the optimum parameters of the model are returned by the algorithm for the specified solar panel. Table 3 displays the values of those five parameters for the three main types of PV panel. To evaluate the accuracy of the different models, the performances of the different models were compared to those of the manufacturer using experimental data obtained from the datasheet of the solar panels. The relative error observed between the voltages for each test point was recorded and displayed in Fig. 8. It was noticed that the maximum relative error was 0.6641%, 0.4072%, and 0.7262% respectively for the type KC200GT, MSX-60, and CS6K-280 M of solar panels. Note that the performance achieved by the single diode model implemented in this paper for the different type of solar panels are very close or better than 0.5% recorded in Ref. [41]. In this aforementioned work, the authors implemented the three diodes model using the sunflower optimization algorithm. It was noticed that the three diodes model achieves a slightly greater accuracy than the single diode model but at the cost of an increase complexity and number of unknown parameters to be identified. The models were further assessed under diverse environmental conditions and compared with experimental data.

Table 2
Parameters of some PV panels at Standard Test Conditions.

Company	Kyocera [52]	Solarex [53]	Canadian Solar [54]
Model	KC200GT	MSX-60	CS6K-280
Cell type (Crystals)	Multi	Poly	Mono
P_m [W]	200	60	280
V_m [V]	26.3	17.1	31.5
I_m [A]	7.61	3.5	8.89
V_{oc} [V]	32.9	21.1	38.5
I_s [A]	8.21	3.8	9.43
N_s [cells]	54	36	60
K_i	0.00318A/°C	0.065%/°C	0.053%/°C
K_v	−0.123V/°C	−0.08V/°C	−0.31%/°C

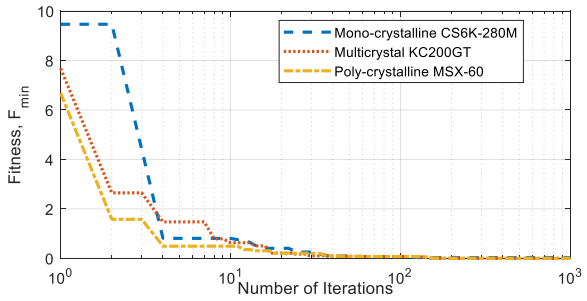

Fig. 7. Fitness function minimization as a function of number of iterations.

Table 3
Unknown parameters determined by PSO for three types of solar panels for Single diode Model.

	Kyocera [52]	Solarex [53]	Canadian Solar [54]
I_{ph} [A]	8.2272	3.8091	9.4376
R_p [Ω]	160.2345	161.0752	349.0997
R_s [Ω] n	0.33535	0.38659	0.2821
	1.0027	0.97359	0.96142
I_s [A]	4.302e-10	2.4515e-10	4.874e-11

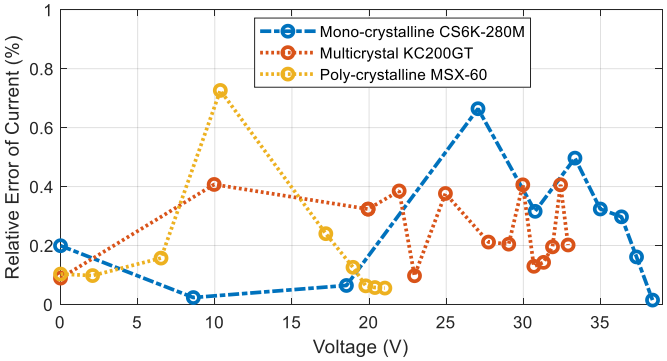

Fig. 8. Relative Error of the solar models based on experimental data.

Two series of tests were done with respect to the different type of commercial PV panels to further assess the accuracy of the model. The first test was carried out under air mass (AM) of 1.5 Pa, constant temperature (T) of 25°C and different irradiance levels (G). The second test was performed at AM = 1.5Pa, G = 1000W/m^2 for various values of the temperature T. Note that for these tests, all the experimental data for the specified conditions are obtained from the datasheet of the manufacturer and superimposed to the curves produced by the various models. Fig. 9 displays the results for these two series of tests performed with the PV panel type KC200GT at different irradiance levels (G) $(1000, 800, 600, 400, 200) W/m^2$ (Fig. 9a) and different temperatures $(25, 50, 75)^\circ C$ (Fig. 9b). It can be seen that the data from the model are in good agreement with those of the manufacturer except at lower irradiance where slight deviations were observed. Fig. 10 displays the results obtained for the PV panel type MSX-60 under different temperature show that the data from the model are in good agreement with those of

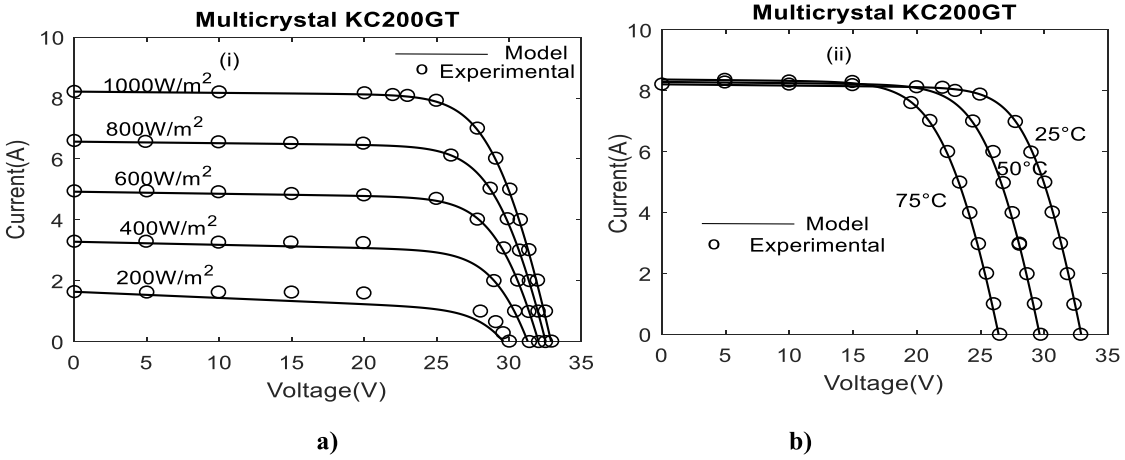

Fig. 9. I–V data of PV panel KC200GT type superimposed to those of the model for different climatic condition (a) Different irradiance levels b) Different temperature levels.

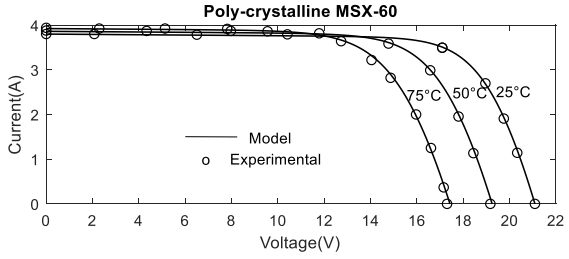

Fig. 10. I–V data of PV panel MSX-60 type superimposed to those of the model at variable temperature.

the manufacturer. Finally, the results of the tests performed with the model CS6K-280 M under varying irradiance and temperatures displayed in Fig. 11 shows that the data of the model curve closely fits the experimental data. In short, the accuracy achieved by single diode model on the three type of solar panels are satisfactory and can be used reliably for the subsequent investigations on MPPT.

6.2. Determination of V_m with ANN

With regards to the calculation of V_m, the ANN introduced in Section 4.1 was trained was trained utilizing 756 distinct environmental conditions encompassing varying degrees of irradiance and temperature in the ranges [0–1000W/m^2] and [0-75 °C]. It is also important to emphasize that the only inputs utilized by this ANN are temperature and voltage (V_{oc}). The voltage is determined using the irradiance-free equation established in Equation (20). Thus, to put it more succinctly, the derived values of G are utilized offline during model training. On the contrary, the online operational measurement of G is circumvented by utilizing Equation (20) and the ANN model.

The neural network designed to determine V_m was trained using Levenberg-Marquardt method. For this purpose, 70% of the dataset is assigned to the training set, while 30% is distributed equally between the validation and testing set. The model was trained for each of the type of solar panels and the algorithm converges at most for the three models after 200 iterations. The mean squared errors obtained for the PV panel types KC200GT, MSX-60, and CS6K-280 M were respectively 1.883×10^{-3}, 6.296×10^{-4}, and 1.773×10^{-3}.

The error was computed as the gap between the estimated (with ANN) and MPP voltage obtained from simulation of the panels in MATLAB Simulink under the same irradiance and temperature values. The mean error recorded was less than 0.212V for all the models. In addition the upper bound ε_b and lower bound ε_a of the errors for each type of PV module were also recorded. The mean error, the upper and lower bound error for each type of PV panel displayed in Table 4 show the level of accuracy achieved in the determination of V_m as the highest gap between upper and lower bound is less than 0.2V which represent a very narrow region where the MPP should be found. This shows that the

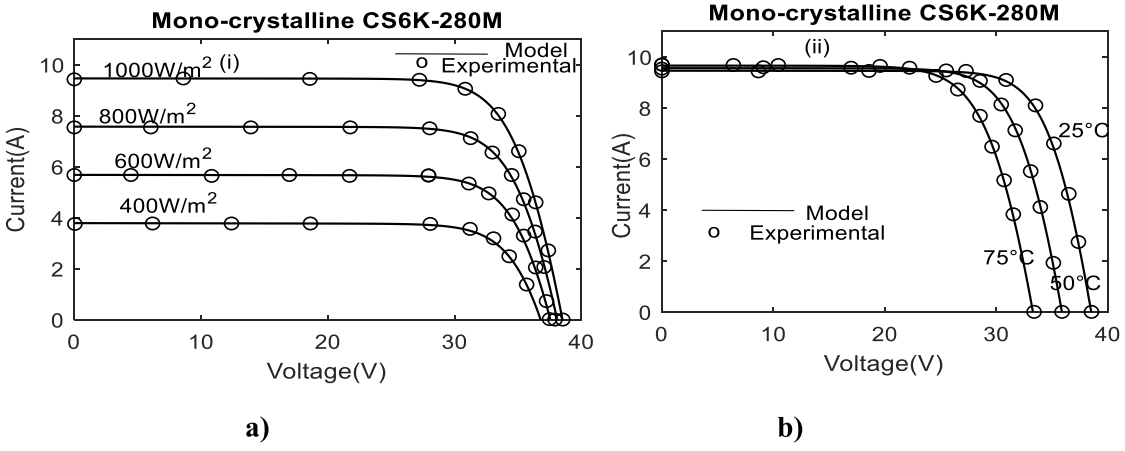

Fig. 11. I–V data of PV panel CS6K-280 M type superimposed to those of the model for different climatic conditions (a) Different irradiance levels b) Different temperature levels.

Table 4
Error analysis of the computed V_m.

PV Module	ε_a (V)	ε_{mean} (V)	ε_b (V)
KC200GT	0.1060	0.1362	0.0872
MSX-60	0.0556	0.2115	0.0427
CS6K-280	0.1103	0.1092	0.0760

proposed computation method can be used to quickly estimate the maximum power voltage V_m for any solar panel. The main asset of this approach is its independence to the measurement of irradiance, unlike the reported methods in the literature as revealed in Table .1. Although all the models exhibit satisfactory performances, only the model with the lowest mean error was considered for subsequent investigations for MPPT improvement. As a result, CS6K-280 was chosen for its highest accuracy and better performance at low solar irradiance conditions.

6.3. Assessment of the proposed MPPT algorithm

To assess the modified MPPT algorithm introduced, several experiment simulations are carried out in order to compare its performances to those of the standard P&O and other methods introduced in the literature based on RSS [28,29]. The different version of the MPPT algorithms are implemented in a boost converter with the following specifications: input capacitance of $720\mu F$, inductance of $10mH$, output capacitance of $87\mu F$, and resistive loads in the range of 10–80 Ω. The constant parameter for robust initialization is set to be 2×10^{-4}, the P&O perturbation step-size of 3×10^{-5} enhanced perturbation step-size for the proposed algorithm 1×10^{-6}. The RSS was defined as a constant space region containing V_m and delimited by the lower and upper bound ε_a, and ε_b respectively as given in Table 4.

The various methods are initially tested with PV module under standard test conditions (1000W/m^2 and 25 °C). The voltage and power curves for each of the methods are displayed in Figs. 12 and 13 respectively. The MPP voltage for this PV module under these conditions is 31.5V (see Fig. 12). It noticed that the P&O and the other two methods [28,29] do not effectively track the MPP voltage. This drawback is due to inadequacy between its perturbation step size to the span of the region where V_m is searched. On the other hand, the subjective assignment of the RSS that is established in the two other methods [28,29] do not always guarantee tracking of the exact MPP voltage. The effect of the RSS is noticeable in the three other algorithms as they exhibit almost no ripple components at steady state in comparison the conventional P&O. To further simplify the discussion of acquired results, let the MPPT algorithm proposed in Ref. [28] be termed Algorithm-A, while that in Ref. [29] be termed Algorithm-B.

Fig. 13 shows that tracking speed the proposed algorithm is 52.73 ms which is faster than of the conventional P&O and the Algorithm-A with respectively 210 ms and 75.7 ms. However, Algorithm-B demonstrates the fastest response because it is not an MPP search algorithm but rather

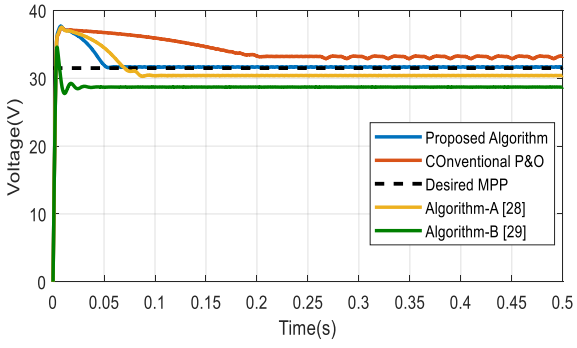

Fig. 12. Voltage of the PV module at STC for different MPPT algorithms: Algorithm-A [28], Algorithm-B [29].

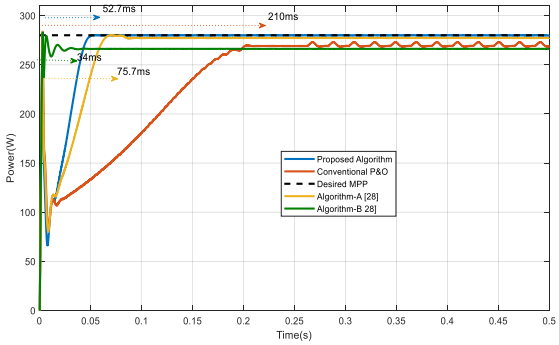

Fig. 13. Power of the PV module at STC for the different MPPT algorithms.

a direct determination of the latter.

The efficiency of the algorithms is computed as the ratio between the PV power and the expected maximum power. It is expressed as:

$$\eta_{mppt} = \frac{P_{pv}}{P_m} \times 100 \tag{25}$$

where P_{pv} is the PV power derived from the panel under the control of the algorithm, P_m is the expected maximum power. In terms of efficiency, it can be clearly noticed from Fig. 13 that the proposed algorithm outperforms the other algorithms with an efficiency of 96.46% as compared to 84.36% of the conventional P&O and 94.68% and 94.83% respectively for algorithms-A and B.

A series of experiments were carried out to assess the delineation of the RSS region with respect to the maximum voltage by Algorithm-A and B using three type of commercial PV panel under various environmental conditions. Using the solar panel KC200GT, the RSS set by algorithms A and B fails to contain the maximum voltage in 40% and 60% of cases respectively for algorithm A and B. This situation grows worst with the two other types of PV panels respectively MSX-60 and CS6K-280 M where in only 30% of the experiments, the defined RSS by two algorithms effectively contain the maximum voltage. This demonstrates that there is no guarantee to find the maximum voltage within RSS when this latter is defined on simplistic assumption. It is obvious that under such conditions, those algorithms cannot track the true MPP and therefore result in limited efficiency. This definitively demonstrates that a precise and systematic determination of the RSS bounds is a crucial step in the improvement of MPPT algorithms.

The proposed algorithm was further assessed under changing environmental conditions and its performances were compared to the algorithms [28,29] including conventional P&O algorithm. For this purpose, a weather profile made up of nine states (S1, …, S9) of equal duration was modeled to simulate the effect of changes in environmental conditions. Each state assumes specific constant irradiance and temperature and all the nine states are presented in Table 5. For this weather profile, the PV voltage and power curves for the different algorithms are displayed in Figs. 14 and 15 respectively. It can be noticed from Fig. 14 that the proposed algorithm effectively track the maximum voltage at every state of the profile with minimal disturbance due to changes in environmental conditions especially during fast transitions.

Fig. 15 shows that the algorithm-A and B demonstrate greater efficiency than the P&O due to their faster response. However, they still do not effectively track the MPP. standard P&O converges to the actual MPP at steady state. In contrast, the proposed algorithm demonstrates effective tracking of the true MPP with higher efficiency compared to the other algorithms. It can be noticed that the proposed algorithm is faster than the standard P&O, and the algorithm-A but it is outperformed by Algorithm-B in terms of tracking time. This is because this algorithm does not search for the MPP but rather estimate the MPP. The efficiency of the algorithms was further compared using the same weather profile and the level of performance achieved in each state by the different

Table 5
Variable Environmental states.

Environmental Conditions	S1	S2	S3	S4	S5	S6	S7	S8	S9
T ($^{\circ}C$)	50	50	20	20	30	30	40	40	10
G(W/m^2)	1000	100	900	700	200	300	500	900	600

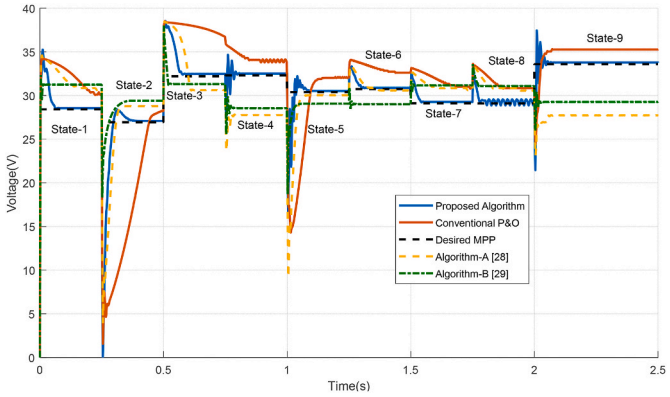

Fig. 14. Voltage of the PV module using the proposed algorithm and other algorithms under varying climatic conditions.

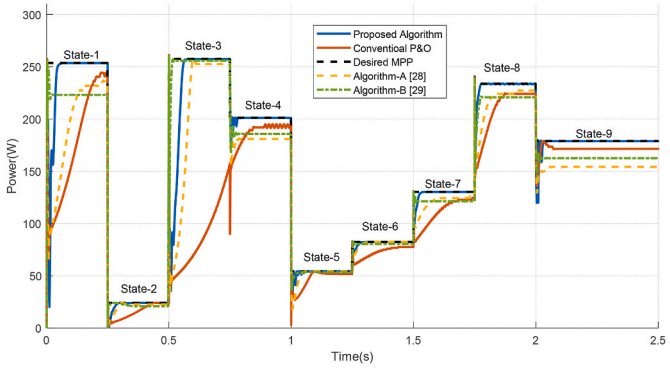

Fig. 15. Power of the PV module of the different algorithms under varying climatic conditions.

algorithms is plotted in Fig. 16. Taking into consideration the nine states, the average efficiency of the standard P&O, Algorithm A, and B are found to be 78.1854%, 86.06% and 92.8307% as compared to the 96.64% for the proposed algorithm. It can be noticed that the proposed algorithm clearly outperforms the other algorithms.

The accelerated response of Algorithm A [29] to climatic conditions is evident from Figs. 13 and 15. The rapid response of this algorithm can be attributed to the fact that, in contrast to the proposed algorithm and other modern algorithms, it does not rely on the pursuit of the MPP.

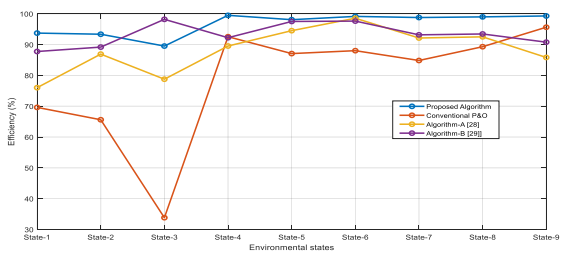

Fig. 16. Efficiency of the different algorithms under varying environmental conditions.

Direct duty cycle determination is utilized, indicating that minimal or no time is spent in the search process. In contrast, the algorithm under consideration is predicated on the pursuit of the MPP. However, it conducts the search operation exclusively within the restricted and constrained search space, in contrast to alternative searching algorithms. Furthermore, in order to enhance the velocity of the proposed algorithm, it is possible to optimize the choice of the robust initialization parameter K_r, which is accountable for accelerating the MPPT operation in its initial stages.

The search space is a vital step for effective determination of the MPP. It is a strategy put forward to surmount the trade-off between tracking speed and steady state oscillations suffered by the standard P&O. In fact, larger step-size fastens the tracking process within the SS, at the expense of steady-state oscillations whereas small step-size reduces the oscillations at the expense of the tracking response speed. Both scenarios are naturally undesired as they contribute in moderating the efficiency of the algorithms. In this paper, it has been demonstrated that it is possible to reduce the search space significantly while ensuring this latter contains the MPP. The implementation of such a strategy to the search space reduction using different type of solar panels including the multi-crystal KC200GT, poly-crystalline MSX-60, and mono-crystalline CS6K-280 M reveals that the new area where the MPP will be searched was reduced to up to 2% of its initial size.

6.4. *Experimental assessment of the proposed MPPT algorithm*

In order to test the consistency of the proposed method, a real-time experiment was set up using the CS6K-280 M solar panel. The experimental test bench, as depicted in Fig. 17, includes the solar panel under investigation, a Pyranometer for measuring solar irradiance, a DHT temperature sensor, a microcontroller unit, and a personal computer equipped with applications for data recording. For this purpose, the irradiance, temperature profiles were recorded for one-daylight duration (from 7:00AM to 6:00PM) as well as the maximum output voltage and power. These same recorded irradiance and temperature profiles as seen in Fig. 18 were fed into the proposed algorithm to compute the MPP voltage and then compare to the experimental one.

Fig. 19 displays the curve of the maximum voltage from experiment and superimposed to the maximum voltage obtained by the proposed method. This plot shows that the estimated V_m consistently agrees with the experimental values throughout the hours of the day, with a concentration of voltage error around 0.1V. The mean error computed as the average gap between the estimated and experimental V_m is found to

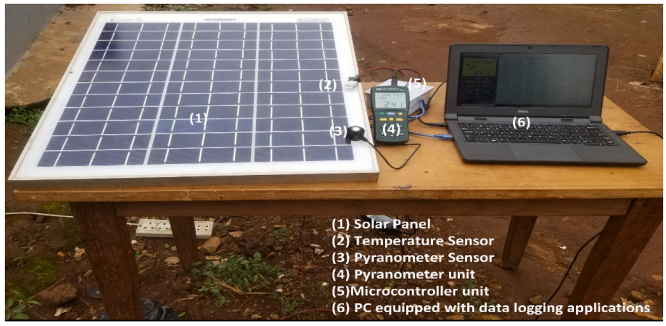

Fig. 17. Experimental setup for Validation.

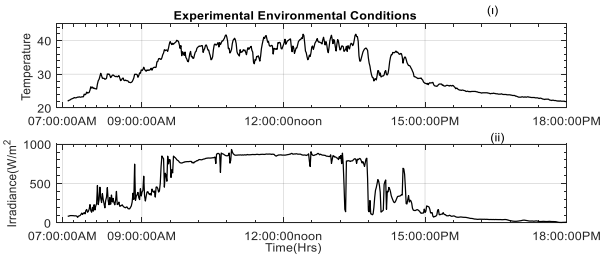

Fig. 18. Experimental climatic measurements.

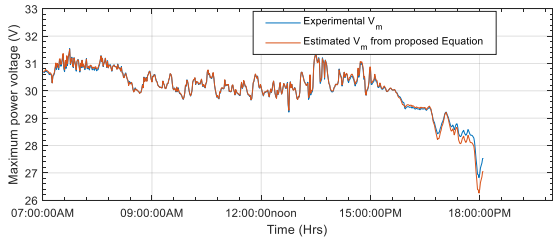

Fig. 19. Plot of the experimental V_m and its estimate using the established equation.

be 0.0128V. The level of error shows that the proposed method is highly accurate and robust to changes in environmental conditions. Nevertheless, it was noticed an increase during the late hours of the day above 5:00PM, with a maximum error of 0.5647V. Such a deviation accounts to the low performance of the one diode model at low solar irradiance values. This experimental results do not only confirm the relevance of the proposed method for MPP estimation, yet it endorses the theoretically constructed profile of irradiance and temperature used to train the model.

Furthermore, to evaluate the effectiveness of the proposed method, the other algorithms [28,29] including the conventional P&O were also tested using the previous recorded irradiance and temperature profiles and their output power were compared to output power of the proposed method. For simulation purpose, the recorded environmental conditions are resampled at a time of 15 min following the procedure of [48], and the simulations are performed in a reduced time frame of 3.5s. The effectiveness of the algorithms is measured by the closeness between its harvested power and the experimental power.

A plot of the experimental power and the PV harvested power using the different MPPT algorithm is displayed in Fig. 20. It is evident that all the MPPT algorithms show a noticeable tracking performance of the experimental power. However, the proposed MPPT algorithm shows the best agreement with the experimental power especially when the PV panel is subject to changes in environmental conditions. This experiment once again, demonstrate the superiority of the proposed method in tracking the MPP as compared to the P&O and the MPPT methods in Refs. [28,29].

7. Conclusion

The electrical energy generated by photovoltaic (PV) panels fluctuates continuously with the surrounding environment and exhibits a nonlinear pattern. The operating point is displaced from the maximum power point (MPP) as a result of these variations, leading to energy loss due to the generated power fluctuating continuously. Maintaining the operating point at the MPP is critical for PV systems to produce the maximum amount of energy. To tackle this issue, the maximum power point tracking (MPPT) algorithm has been devised. Nevertheless, the numerous MPPT algorithms that have been documented thus far encounter numerous obstacles, including a sluggish tracking response and only average efficiency. These constraints stem from the fact that the MPP conducts searches across a broad search space area.

An exhaustive methodology was devised in this article to decrease the search area of the MPP with the intention of enhancing the performance of the MPPT algorithms. Three prevalent categories of solar panels—KC200GT, Poly-Crystalline MSX-60, and Mono-crystalline CS6K-280M—were utilized in order to ascertain the unidentified parameters of a PV panel's single diode model through the implementation of a hybrid analytical and particle swarm optimization algorithm. The evaluation of the models was conducted through a comparison with benchmark data. The maximum relative error observed for the solar panel types KC200GT, MSX-60, and CS6K-280 M was 0.6641%, 0.4072%, and 0.7262%, respectively. An estimation of the MPP voltage was performed by a simple neural network with a hidden layer consisting of two inputs and temperature (open circuit voltage and temperature) using the precise single diode model previously developed. The experimental results obtained from the implementation of this ANN demonstrated its capability to precisely estimate the MPP voltage, with upper and lower limits of error of 0.106V and 0.0872V, respectively. Following this, the upper and lower limits were implemented to delineate the search space's boundary. The application of search space reduction to a prevalent solar type indicates that the initial size of the newly delineated area for the MPP search was diminished by as little as 2%.

Aware that the primary limitation of certain pre-existing algorithms and the standard P&O algorithm is the requirement for a substantial or intuitively defined search space to locate the target MPP, the conventional P&O algorithm was modified to incorporate the proposed search space strategy. For a robust initialization, the algorithm first rapidly estimates the MPP voltage, and then employs the search space strategy introduced to precisely locate the true MPP voltage in a reduced number

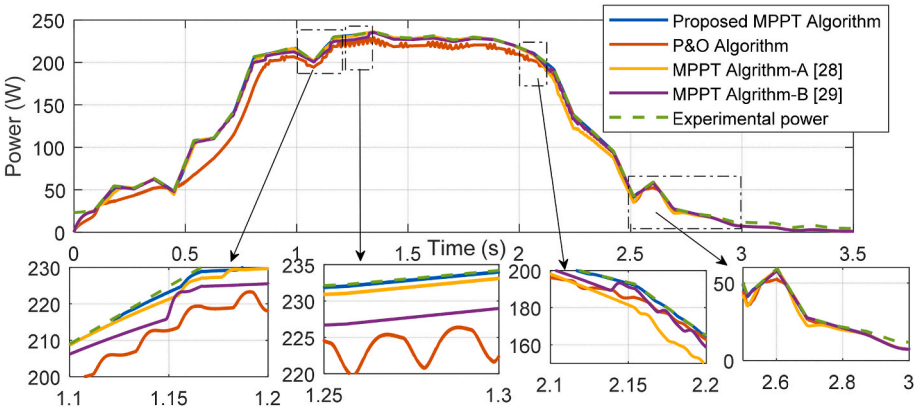

Fig. 20. PV power extracted by different MPPT algorithms using real-time data.

of steps. A sequence of simulations conducted to evaluate the proposed method revealed a significant improvement in the speed and efficiency of maximal power point tracking. Moreover, under diverse environmental conditions, it was unequivocally demonstrated that the proposed method outperforms the standard P&O and several comparable confinement-based algorithms [[28,29]]. One of the primary directions for future research entails augmenting the current investigation to encompass PV systems operating in partial shading conditions. Moreover, approaches for enhancing the efficacy of MPPT can be found in the optimization of the robust initialization parameter K_τ.

CRediT authorship contribution statement

Ambe Harrison: Conceptualization, Data curation, Formal analysis, Investigation, Methodology, Software, Visualization, Writing – original draft. **Cyrille Feudjio:** Data curation, Methodology, Project administration, Resources, Supervision, Validation, Visualization, Writing – review & editing. **Christophe Raoul Fotso Mbobda:** Formal analysis, Visualization, Writing – review & editing. **Njimboh Henry Alombah:** Data curation, Investigation, Visualization, Writing – review & editing.

Declaration of competing interest

The authors declare that they have no known competing financial interests or personal relationships that could have appeared to influence the work reported in this paper.

Data availability

No data was used for the research described in the article.

References

[1] P.A. Owusu, S. Asumadu-Sarkodie, A review of renewable energy sources, sustainability issues and climate change mitigation, Cogent Eng 3 (2016) 1167990, https://doi.org/10.1080/23311916.2016.1167990.

[2] D. Welsby, J. Price, S. Pye, P. Ekins, Unextractable fossil fuels in a 1.5 °C world, Nature 597 (2021) 230–234, https://doi.org/10.1038/s41586-021-03821-8.

[3] M.Z. Jacobson, M.A. Delucchi, M.A. Cameron, B.V. Mathiesen, Matching demand with supply at low cost in 139 countries among 20 world regions with 100% intermittent wind, water, and sunlight (WWS) for all purposes, Renew. Energy 123 (2018) 236–248, https://doi.org/10.1016/j.renene.2018.02.009.

[4] A. Sadiqa, A. Gulagi, C. Breyer, Energy transition roadmap towards 100% renewable energy and role of storage technologies for Pakistan by 2050, Energy 147 (2018) 518–533, https://doi.org/10.1016/j.energy.2018.01.027.

[5] A.G. Olabi, M.A. Abdelkareem, Renewable energy and climate change, Renew. Sustain. Energy Rev. 158 (2022) 112111, https://doi.org/10.1016/j.rser.2022.112111.

[6] S. Reichelstein, M. Yorston, The prospects for cost competitive solar PV power, Energy Pol. 55 (2013) 117–127, https://doi.org/10.1016/j.enpol.2012.11.003.

[7] H. Lin, M. Yang, X. Ru, G. Wang, S. Yin, F. Peng, C. Hong, M. Qu, J. Lu, L. Fang, C. Han, P. Procel, O. Isabella, P. Gao, Z. Li, X. Xu, Silicon heterojunction solar cells with up to 26.81% efficiency achieved by electrically optimized nanocrystalline-silicon hole contact layers, Nat. Energy (2023), https://doi.org/10.1038/s41560-023-01255-2.

[8] A.F. Tchouani Njomo, G. Kenne, R.M. Douanla, L.L. Sonfack, A modified ESC algorithm for MPPT applied to a photovoltaic system under varying environmental conditions, Int. J. Photoenergy 2020 (2020) 1–15, https://doi.org/10.1155/2020/1956410.

[9] T. Esram, P.L. Chapman, Comparison of photovoltaic array maximum power point tracking techniques, IEEE Trans. Energy Convers. 22 (2007) 439–449, https://doi.org/10.1109/TEC.2006.874230.

[10] P. Bhatnagar, R.K. Nema, Maximum power point tracking control techniques: state-of-the-art in photovoltaic applications, Renew. Sustain. Energy Rev. 23 (2013) 224–241, https://doi.org/10.1016/j.rser.2013.02.011.

[11] A. Reza Reisi, M. Hassan Moradi, S. Jamasb, Classification and comparison of maximum power point tracking techniques for photovoltaic system: a review, Renew. Sustain. Energy Rev. 19 (2013) 433–443, https://doi.org/10.1016/j.rser.2012.11.052.

[12] M.A. Eltawil, Z. Zhao, MPPT techniques for photovoltaic applications, Renew. Sustain. Energy Rev. 25 (2013) 793–813, https://doi.org/10.1016/j.rser.2013.05.022.

[13] N. Femia, G. Petrone, G. Spagnuolo, M. Vitelli, Optimization of perturb and observe maximum power point tracking method, IEEE Trans. Power Electron. 20 (2005) 963–973, https://doi.org/10.1109/TPEL.2005.850975.

[14] S. Salman, X. Ai, Z. Wu, Design of a P-& -O algorithm based MPPT charge controller for a stand-alone 200W PV system, Prot. Control Mod. Power Syst. 3 (2018) 25, https://doi.org/10.1186/s41601-018-0099-8.

[15] R. Alik, A. Jusoh, Modified Perturb and Observe (P& O) with checking algorithm under various solar irradiation, Sol. Energy 148 (2017) 128–139, https://doi.org/10.1016/j.solener.2017.03.064.

[16] A. Al-Diab, C. Sourkounis, Variable step size P& O MPPT algorithm for PV systems, in: 2010 12th Int. Conf. Optim. Electr. Electron. Equip., IEEE, 2010, pp. 1097–1102, https://doi.org/10.1109/OPTIM.2010.5510441.

[17] X. Li, H. Wen, C. Zhao, Improved beta parameter based MPPT method in photovoltaic system, in: 2015 9th Int. Conf. Power Electron. ECCE Asia (ICPE-ECCE Asia), IEEE, 2015, pp. 1405–1412, https://doi.org/10.1109/ICPE.2015.7167963.

[18] X. Li, H. Wen, Y. Hu, L. Jiang, W. Xiao, Modified beta algorithm for GMPPT and partial shading detection in photovoltaic systems, IEEE Trans. Power Electron. 33 (2018) 2172–2186, https://doi.org/10.1109/TPEL.2017.2697459.

[19] K.-H. Chao, M.N. Rizal, A hybrid MPPT controller based on the genetic algorithm and Ant Colony optimization for photovoltaic systems under partially shaded conditions, Energies 14 (2021) 2902, https://doi.org/10.3390/en14102902.

[20] T. Radjai, J.P. Gaubert, L. Rahmani, S. Mekhilef, Experimental verification of P& O MPPT algorithm with direct control based on Fuzzy logic control using CUK converter, Int. Trans. Electr. Energy Syst. 25 (2015) 3492–3508, https://doi.org/10.1002/etep.2047.

[21] U. Yilmaz, O. Turksoy, A. Teke, Improved MPPT method to increase accuracy and speed in photovoltaic systems under variable atmospheric conditions, Int. J. Electr. Power Energy Syst. 113 (2019) 634–651, https://doi.org/10.1016/j.ijepes.2019.05.074.

[22] X. Li, Q. Wang, H. Wen, W. Xiao, Comprehensive Studies on Operational Principles for Maximum Power Point Tracking in Photovoltaic Systems, IEEE Access, 2019, p. 1, https://doi.org/10.1109/ACCESS.2019.2937100.

[23] J. Macaulay, Z. Zhou, A fuzzy logical-based variable step size P& O MPPT algorithm for photovoltaic system, Energies 11 (2018) 1340, https://doi.org/10.3390/en11061340.

[24] M.H. Osman, A. Refaat, Adaptive multi-variable step size P& O MPPT for high tracking-speed and accuracy, IOP Conf. Ser. Mater. Sci. Eng. 643 (2019) 012050, https://doi.org/10.1088/1757-899X/643/1/012050.

[25] L.P. Jyothy, M.R. Sindhu, An artificial neural network based MPPT algorithm for solar PV system, in: 2018 4th Int. Conf. Electr. Energy Syst., IEEE, 2018, pp. 375–380, https://doi.org/10.1109/ICEES.2018.8443277.

[26] A. Harrison, N.H. Alombah, J. de Dieu Nguimfack Ndongmo, A new hybrid MPPT based on incremental conductance-integral backstepping controller applied to a PV system under fast-changing operating conditions, Int. J. Photoenergy 2023 (2023) 1–17, https://doi.org/10.1155/2023/9931481.

[27] S.D. Al-Majidi, M.F. Abbod, H.S. Al-Raweshidy, A particle swarm optimisation-trained feedforward neural network for predicting the maximum power point of a photovoltaic array, Eng. Appl. Artif. Intell. 92 (2020) 103688, https://doi.org/10.1016/j.engappai.2020.103688.

[28] M. Kamran, M. Mudassar, M.R. Fazal, M.U. Asghar, M. Bilal, R. Asghar, Implementation of improved Perturb & Observe MPPT technique with confined search space for standalone photovoltaic system, J. King Saud Univ. - Eng. Sci. 32 (2020) 432–441, https://doi.org/10.1016/j.jksues.2018.04.006.

[29] A. Chellakhi, S. El Beid, Y. Abouelmahjoub, Implementation of a Novel MPPT Tactic for PV System Applications on MATLAB/Simulink and Proteus-Based Arduino Board Environments, 2021, p. 2021.

[30] R. Iftikhar, I. Ahmad, M. Arsalan, N. Naz, N. Ali, H. Armghan, MPPT for photovoltaic system using nonlinear controller, Int. J. Photoenergy (2018) 1–11, https://doi.org/10.1155/2018/6979723, 2018.

[31] A. Aldosary, Z.M. Ali, M.M. Alhaider, M. Ghahremani, S. Dadfar, K. Suzuki, A modified shuffled frog algorithm to improve MPPT controller in PV System with storage batteries under variable atmospheric conditions, Control Eng. Pract. 112 (2021) 104831, https://doi.org/10.1016/j.conengprac.2021.104831.

[32] M. Jiang, M. Ghahremani, S. Dadfar, H. Chi, Y.N. Abdallah, N. Furukawa, A novel combinatorial hybrid SFL–PS algorithm based neural network with perturb and observe for the MPPT controller of a hybrid PV-storage system, Control Eng. Pract. 114 (2021) 104880, https://doi.org/10.1016/j.conengprac.2021.104880.

[33] H. Tao, M. Ghahremani, F.W. Ahmed, W. Jing, M.S. Nazir, K. Ohshima, A novel MPPT controller in PV systems with hybrid whale optimization-PS algorithm based ANFIS under different conditions, Control Eng. Pract. 112 (2021) 104809, https://doi.org/10.1016/j.conengprac.2021.104809.

[34] A. Harrison, N.H. Alombah, J. de Dieu Nguimfack Ndongmo, Solar irradiance estimation and optimum power region localization in PV energy systems under partial shaded condition, Heliyon 9 (2023) e18434, https://doi.org/10.1016/j.heliyon.2023.e18434.

[35] E. Korany, D. Yousri, H.A. Attia, A.F. Zobaa, D. Allam, A novel optimized dynamic fractional-order MPPT controller using hunter pray optimizer for alleviating the tracking oscillation with changing environmental conditions, Energy Rep. 10 (2023) 1819–1832, https://doi.org/10.1016/j.egyr.2023.08.038.

[36] K. Ullah, M. Ishaq, F. Tchier, H. Ahmad, Z. Ahmad, Fuzzy-based maximum power point tracking (MPPT) control system for photovoltaic power generation system, Results Eng 20 (2023) 101466, https://doi.org/10.1016/j.rineng.2023.101466.

[37] M. said Adouairi, B. Bossoufi, S. Motahhir, I. Saady, Application of fuzzy sliding mode control on a single-stage grid-connected PV system based on the voltage-oriented control strategy, Results Eng 17 (2023) 100822, https://doi.org/10.1016/j.rineng.2022.100822.

[38] D. Kumar, Y.K. Chauhan, A.S. Pandey, A.K. Srivastava, V. Kumar, F. Alsaif, R. M. Elavarasan, M.R. Islam, R. Kannadasan, M.H. Alsharif, A novel hybrid MPPT approach for solar PV systems using particle-swarm-optimization-trained machine

learning and flying Squirrel search optimization, Sustainability 15 (2023) 5575, https://doi.org/10.3390/su15065575.
[39] R. Ayop, C.W. Tan, Design of boost converter based on maximum power point resistance for photovoltaic applications, Sol. Energy 160 (2018) 322–335, https://doi.org/10.1016/j.solener.2017.12.016.
[40] I. Glasner, J. Appelbaum, Advantage of boost vs. buck topology for maximum power point tracker in photovoltaic systems, in: Proc. 19th Conv. Electr. Electron. Eng. Isr., IEEE, n.d.: pp. 355–358. https://doi.org/10.1109/EEIS.1996.566988.
[41] M.H. Qais, H.M. Hasanien, S. Alghuwainem, Identification of electrical parameters for three-diode photovoltaic model using analytical and sunflower optimization algorithm, Appl. Energy 250 (2019) 109–117, https://doi.org/10.1016/j.apenergy.2019.05.013.
[42] K. Yu, B. Qu, C. Yue, S. Ge, X. Chen, J. Liang, A performance-guided JAYA algorithm for parameters identification of photovoltaic cell and module, Appl. Energy 237 (2019) 241–257, https://doi.org/10.1016/j.apenergy.2019.01.008.
[43] J. Zhou, Y. Zhang, Y. Zhang, W.-L. Shang, Z. Yang, W. Feng, Parameters identification of photovoltaic models using a differential evolution algorithm based on elite and obsolete dynamic learning, Appl. Energy 314 (2022) 118877, https://doi.org/10.1016/j.apenergy.2022.118877.
[44] S. Lidaighbi, M. Elyaqouti, D. Ben Hmamou, D. Saadaoui, K. Assalaou, E. Arjdal, A new hybrid method to estimate the single-diode model parameters of solar photovoltaic panel, Energy Convers. Manag. X. 15 (2022) 100234, https://doi.org/10.1016/j.ecmx.2022.100234.
[45] J. Kennedy, R. Eberhart, Particle swarm optimization, in: Proc. ICNN'95 - Int. Conf. Neural Networks, IEEE, 1942–1948, https://doi.org/10.1109/ICNN.1995.488968 n.d.: pp.
[46] H.-P. Dai, D.-D. Chen, Z.-S. Zheng, Effects of random values for particle swarm optimization algorithm, Algorithms 11 (2018) 23, https://doi.org/10.3390/a11020023.
[47] M.T. Penella, M. Gasulla, A simple and efficient MPPT method for low-power PV cells, Int. J. Photoenergy 2014 (2014) 1–7, https://doi.org/10.1155/2014/153428.
[48] A. Hassan, O. Bass, M.A.S. Masoum, An improved genetic algorithm based fractional open circuit voltage MPPT for solar PV systems, Energy Rep. 9 (2023) 1535–1548, https://doi.org/10.1016/j.egyr.2022.12.088.
[49] V.J. Chin, Z. Salam, K. Ishaque, An improved method to estimate the parameters of the single diode model of photovoltaic module using differential evolution, in: 2015 4th Int. Conf. Electr. Power Energy Convers. Syst., IEEE, 2015, pp. 1–6, https://doi.org/10.1109/EPECS.2015.7368514.
[50] B. Li, C. Delpha, D. Diallo, A. Migan-Dubois, Application of Artificial Neural Networks to photovoltaic fault detection and diagnosis: a review, Renew. Sustain. Energy Rev. 138 (2021) 110512, https://doi.org/10.1016/j.rser.2020.110512.
[51] V.S.S. Vankayala, N.D. Rao, Artificial neural networks and their applications to power systems—a bibliographical survey, Electr. Power Syst. Res. 28 (1993) 67–79, https://doi.org/10.1016/0378-7796(93)90081-O.
[52] Kyocera, KC200GT Kyocera PV Module Datasheet, 2018 n.d. https://www.solarelectricsupply.com/kyocera-kc200gt-solar-panel. (Accessed 10 April 2023).
[53] Solarex, MSX-60 PV Module Solarex Datasheet, 2018. Online. (n.d.), https://www.solarelectricsupply.com/solar-panels/solarex/solarex-msx-60-w-junction-box. (Accessed 10 April 2023).
[54] CS6K-280M canadiansolar PV module datasheet., (n.d.). https://www.canadiansolar.com/.